DOI: 10.1007/s00382-017-3772-0

Enhanced seasonal predictability of the summer mean temperature in Central Europe favored by new dominant weather patterns

P. Hoffmann

the date of receipt and acceptance should be inserted later

Abstract In this study two complementary approaches have been combined to estimate the reliability of the data-driven seasonal predictability of the meteorological summer mean temperature (T_{JJA}) over Europe. The developed model is based on linear regressions and uses early season predictors to estimate the target value T_{JJA}. We found for the Potsdam (Germany) climate station that the monthly standard deviations (σ) from January to April and the temperature mean (m) in April are good predictors to describe T_{JJA} after 1990. However, before 1990 the model failed. The core region where this model works is the north-eastern part of Central Europe.
We also analyzed long-term trends of monthly *Hess/Brezowsky* weather types as possible causes of the dynamical changes. In spring, a significant increase of the occurrences for two opposite weather patterns was found: *Zonal Ridge across Central Europe* (BM) and *Trough over Central Europe* (TRM). Both currently make up about 30% of the total alternating weather systems over Europe. Other weather types are predominantly decreasing or their trends are not significant. Thus, the predictability may be attributed to these two weather types where the difference between the two Z500 composite patterns is large. This also applies to the north-eastern part of Central Europe.
Finally, the detected enhanced seasonal predictability over Europe is alarming, because severe side effects may occur. One of these are more frequent climate extremes in summer half-year.

1 Introduction

In the age of rapid climate change and the associated increase of extreme record-breaking weather events (e.g. Lehmann et al, 2015; Coumou et al, 2013), it is more important than ever to identify potential risks at an early stage. One crucial question in this context is, whether there are any early season predictors for mean circulation conditions which favor one of these extremes. Most of these extremes occurring at Northern Hemisphere mid-latitudes (e.g.the European heat wave in 2003, the Russian heat wave 2010, the Pakistan flood 2010 and the heat wave in the United States in 2011) can be linked to resonant Rossby waves (Petoukhov et al, 2013). Such a wave mechanism behind those climate extremes increases the chance of a longer-term predictability of the general atmospheric conditions on the seasonal timescale. For example, a seasonal prediction of the summer mean temperature state over Europe could be a predictor for wet, dry or heat conditions. A systematic observational data analysis, which considers the linkage across seasons, would provide valuable information about the natural state of the atmosphere and its predictability. Similar approaches are already commonly used in climate relevant sectors, for example, agriculture to estimate crop yields before sowing in certain regions using atmosphere or SST patterns as early season predictors in regression models (e.g. Jarlan et al, 2014). For instance, circulation patterns over the North-Atlantic sector are linked to the precipitation variability in Morocco (Knippertz et al, 2003) and consequently affect the growing season there. Such a possible way applied to climatic target variables is described in this paper.
Long-term daily time series of meteorological observations include a wide range of information about the state and variability of the global, regional and local climate system. As an introduction into the later presented methods we show two operationally performed analyses of the daily mean 2m-temperature values recorded at the Potsdam secular station. First, a regime shift around 1980 is visible by calculating the monthly standard deviations. Figure 1 depicts a strong decline of the late winter variability (February-March) after 1960 which occurs in synchrony with a rising summer variability (June-July). In the 1980s both reach the same magnitude. During the last decades a synchronization between the winter and summer variability was found. Furthermore, the variability in the transition season (April-May) jumped up to a rather stable state from 1990 to date.

Second, the relation between the proxies for the state and the variability using *first differences* ($\triangle^1$) of the *monthly means* (m) and *monthly standard deviations* (σ) derived from the same temperature record is represented in Fig.2. It shows the correlation between the individual monthly time series of m vs. σ to each other. An area of positive coefficients

Potsdam Institute for Climate Impact Research, P.O. Box 60 12 03, 14412 Potsdam

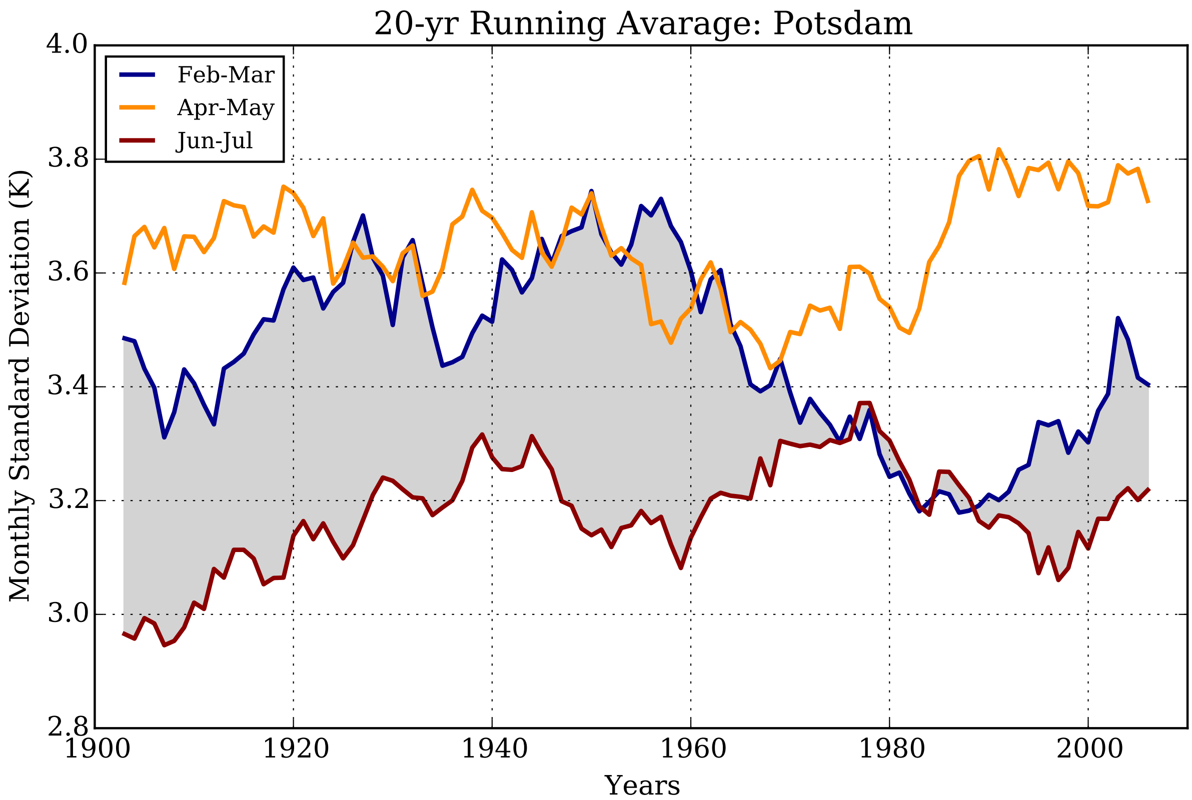

Fig. 1 20-year running mean time series of the monthly standard deviation averaged over two months periods: Feb-Mar (blue), Apr-May (green) and Jun-Jul (orange).

is found in the center of every contour panel for the past period (1951-1980) and the recent period (1986-2015). In the transition from spring to summer we found high correlations between $m\{T_{Apr}\}$ and $\sigma\{T_{May}\}$, $m\{T_{May}\}$ and $\sigma\{T_{Jun}\}$ as well as between $m\{T_{Jun}\}$ and $\sigma\{T_{Jul}\}$. Under recent conditions this structure is stronger surrounded by areas of anti-correlations than under past conditions. The both preliminary analyses show first indications for a stronger dynamical linkage across seasons.

In order to substantiate this fact two complementary approaches will be combined to identify possible changes in the seasonal predictability. First, an univariate regression model was used to estimate the target value in the middle of a year. The summer mean temperature (T_{JJA}) was chosen due to its great social and economic relevance across sectors, such as tourism, public health, plant productivity, etc. As early season predictors a set of temperature derived variability measures for the first months of a year was composed (see Section 2). Second, we apply this approach to the regional scale (Europe) and combine this step with a weather pattern analysis in order to identify potential coincidences.

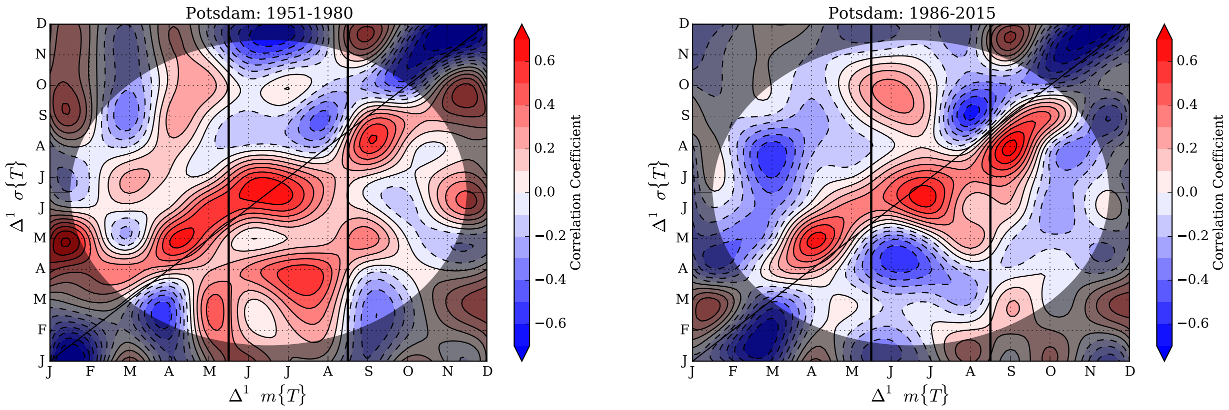

Fig. 2 Monthly Pearson correlation coefficient matrix between $m\{T\}$ end $\sigma\{T\}$ using $\triangle^1$ from 1951-1980 (left) and 1986-2015 (right) in Potsdam. The area of interest is highlighted.

More complex empirical models (e.g. Rust et al, 2015; Eden et al, 2015) are not sufficient for this task. These are often based on multiple linear regression, using a mixed set of independent early predictors (e.g. teleconnection indices) to estimate a target value in the near future. Thus, the results cannot be clearly attributed to one source. Furthermore, with these complex models long-term analyses over about one century are not feasible due to the lack of homogeneous data. Both issues are solved in our combined approach. Certainly, for more comprehensive investigations, further analysis techniques, such as Principle Component Analysis (e.g. Barnett et al, 1984; Stock and Watson, 2002; Della-Marta et al, 2007), Partial Least-Square regression (e.g. Wold et al, 2001; Smoliak et al, 2010) or Wavelet regression (e.g. Prokoph and Patterson, 2004) could provide additional benefits, because atmospheric or oceanic patterns can be considered. In the medium term the combination of process-based operationally forecasts, e.g. CFS (Saha and Coauthors, 2014) or IRI (Barnston and Mason, 2011) and data-driven approaches (as presented here) could contribute to more skillful assessments of seasonal predictions.

In this paper we address, how far the regional climate over Europe becomes more predictable during the last decades. In order to answer this question we combine two complementary methods, namely (1) identify the seasonal predictability changes and we (2) explain these by shifting dynamics.

2 Data and Methods

The basic idea of this study is to setup a quasi univariate empirical prediction model to estimate the meteorological summer mean temperature (T_{JJA}) in a time series and one parameter several months in advance. Already, Colman and Davey (1999) found a predictive relationship between the North-Atlantic SST anomalies in winter and the subsequent summer temperature (July-August) in Central England. In this approach the daily temperature record is aggregated to monthly means (m) and standard deviations (σ) describing the state and variability, respectively. The target value (T_{JJA}) will be estimated by a linear combination of early season predictors. The monthly standard deviations from January to April and the temperature state in April are used in our approach:

$$T_{JJA} = const. + a \cdot \sigma\left(T_{Jan}\right) + b \cdot \sigma\left(T_{Feb}\right) + c \cdot \sigma\left(T_{Mar}\right) + d \cdot \sigma\left(T_{Apr}\right) + e \cdot m\left(T_{Apr}\right) + err \tag{1}$$

Those are intended to approximate (1) the low frequency fluctuations over Europe in the first 4 months of a year and (2) the adjusted phase in mid-spring. A strong contribution of the monthly mean temperature in April to the target value is expected. The individual components are detrended using first order differences ($\triangle^1$) as suggested by Gornott and Wechsung (2016) and the system is solved using the Ordinary Least Squares (OLS) method. Former describes the particular states with respect to the previous years. In order to assess the predictability the squared correlation coefficient (r^2) between the observed and modeled values is calculated. This measure is also used to monitor the long-term behavior. All used numerical and graphical libraries are standard Python packages (numpy, matplotlib).

The set of predictors in Eq.1 were found by a visual interpretation of Fig.2 (right panel). It shows the correlation matrix between monthly means (m) and monthly standard deviations (σ) for the present climate at Potsdam. The individual values are detrended by first differences (Δ^1). By considering the monthly means in summer an anticorrelation to the standard deviations in January, February, March and April is found. On the other hand, by considering the monthly standard deviations in summer an anticorrelation to the monthly means in April or May is evident. The monthly standard deviations in the summer months are correlated to monthly means in summer (red cluster in the center). Consequently, the early season predictors for the regression model (Eq.1) can be narrowed. An additional sensitivity analysis was applied to check the model performance, respectively.

The physical concept behind this empirical model is to approximate the amplitude and phase of the low-frequency fluctuations in the transition from the winter to the spring season on the local level. The main drivers are planetary waves moving around the globe at Northern Hemisphere mid-latitudes. They have characteristic properties: zonal wave number and phase speed. The long-term development of the meridional temperature gradient and the land-ocean temperature contrast change their behavior (e.g. Molteni et al, 2011). On the regional level (e.g. Europe) the phase positions of these global scale waves form patterns which are synoptically interpreted as different weather types. It exists a multitude of shapes of the circulation. It is expected, that specific properties of the variability from January to April favor a certain behavior of the summer season, due to a more regular sequence of dominant weather types. Wave-like circulation patterns such as troughs or ridges over Central Europe are possible candidates. This is further analyzed in Section 3.4

In this study the model has been applied to different daily temperature datasets. For the local and long-term inspection the Potsdam climate station was analyzed from 1893 to 2015 (Section 3.1). For the regional view on the European domain the EOBS-0.25-v12 (Haylock et al, 2008) from 1950 to 2015 (Section 3.2) and the surface temperature in NCEP/NCAR R1 reanalysis data (Kalnay and et al., 1996) are used (Fig.15). Finally, the dynamical interpretation of the results is based on a subjectively derived classification of weather types by Hess and Brezowsky (1977), provided by the German Meteorological Service under (http://www.dwd.de/DE/leistungen/grosswetterlage/), see Section 3.4.

The respective composite patterns for the dominant weather types (Fig.9) are extracted from Z500 NCEP/NCAR R1 (Kalnay and et al., 1996) reanalysis fields for dates classified as TRM and dates classified as BM, respectively, in order to interpret their large scale circulation characteristics.

Furthermore, a Mother-Wavelet analysis (Torrence and Compo, 1998) is used to analyze the difference between two period spectra. This approach is also used to low-pass filter temperature fluctuations.

Finally, the results obtained by the regression model (Eq.1) are compared to the performance of the Partial-Least-Squares (PLS) regression (e.g. Geladi and Kowalski, 1986; Smoliak et al, 2010) approach. The procedure calculates the correlation coefficient between the target value ($\Delta^1 T_{JJA}$) and the early season predictors ($\Delta^1 Z500_{FMA}$) over the Atlantic-European sector. By using a Least-Square fitting the individual $\Delta^1 Z500$ patterns are projected onto the correlation matrix. This step is repeated many times for the residuals. The resulting predictor time series of the leading components can used for the prediction.

3 Results & Discussions

3.1 Local (Potsdam)

The model is firstly applied using a long-term daily temperature record at a Central European climate station. One of the longest and most homogeneous record with missing data on only one day since 1893 is the secular station at Potsdam (52.2°N/13.4°E). Setting up the regression model (Eq.1) using the data from 1981 to 2014 the resulted output statistics is given in Tab.1. The fitted and adjusted R-square (r^2, d^2) was 0.45 and 0.35, respectively. All regression coefficients ($a \ldots e$) are negative, which means that a low variability in late winter and a cold April compared to the previous year are good indicators for a positive summer mean temperature $\triangle^1$. The most significant contributions deliver $\sigma\left\{T_{Feb}\right\}$, $\sigma\left\{T_{Mar}\right\}$, $m\left\{T_{Apr}\right\}$ having probability values $p \leq 0.05$. All other non-significant predictors included in this model contribute to better resolve single peaks more precisely. For instance, at the Potsdam climate station the mean temperature in April was 12.0°C (2014) and 9.3°C (2015). A first difference of -2.7K multiplied by the coefficient -0.40 (mApr) results in a +1.08K temperature increase of the summer 2015 when compared to the summer 2014.

Table 1 Ordinary Least Squares model output statistics for Fig.3 (1981-2014).

variable	const.	σJan	σFeb	σMar	σApr	mApr
coefficient	0.12	-0.11	-0.29	-0.38	-0.20	-0.40
std. error	0.22	0.14	0.15	0.21	0.17	0.11
t-statistic	0.52	-0.79	-2.02	-1.87	-1.17	-3.67
p-value	0.61	0.44	0.05	0.07	0.25	0.00
model statistics						
R-squared						0.4459
adjusted R-squared						0.3469
F-statistic						4.5061
prob .(F-statistic)						0.0039
log likelihood						-53.6984
AIC criterion						3.5117
BIC criterion						3.7810

Figure 3 shows the time series of the observed summer mean temperature values (first differences: $\triangle^1$) in Potsdam from 1981 to 2014 (solid line) and the modeled one (dashed line). The regression model applied to the set of indicators revealed a good correspondence to the observed behavior given by $r^2 = 0.45$. The RMSE was 1.2K compared to the total range of 6.8K. Except for 1984 and 2003 all years agree in sign. The summer 2003 was characterized by an extended heat wave. This year is somewhat underestimated by the model. Träger-Chatterjee et al (2014) analyzed atmospheric precursors of this event and found specific conditions during the transition from winter to spring, however, no evidence for an interlink between the North Atlantic Oscillation (NAO) or the Arctic Oscillation (AO) and the heat summer was found. The underrepresentation of this event in the model can be addressed to the usage of first differences ($\triangle^1$). Without it the predictability measure would reach lower values and the miscalculation of 2003 would be less pronounced. A shortening of the training period improved the predictability up to $r^2 = 0.6$ (as shown in Fig.6) and reduced the stability.

The meteorological summer mean temperature in 2015 (see Fig.3) was predicted by applying the regression coefficients to the new observed set of the 5 monthly indicators, respectively. An one out-of-sample cross-validation resulted in a low uncertainty range for the target value (red circles) of about ±0.2K. Converted into absolute values the prediction for the T_{JJA} 2015 was 19.3°C and hence 1.1K warmer than 2014. In the course of the summer of 2015 the monthly means were gradually recorded (green scatter). Finally, the observed summer mean temperature 2015 in Potsdam reached 19.3°C (green circle). This is exactly the predicted one. However, the prediction seemed to fail after the first two summer months June and July (green triangles). These monthly means lay below the previous ones. An extended heat wave over Central Europe in the first half of August 2015 (green square) could compensate the prognostic temperature deficit and a new monthly mean temperature record was reported. The hottest August (1997) with 21.2°C by then was exceeded by 0.6K. August 2015 was with 21.8°C the hottest one since 1893 and 4.6K above the climate normal (1961-1990). Altogether 13 hot days ($T_{max} > 30$°C) and 4 tropical nights ($T_{min} > 20$°C) were reported.

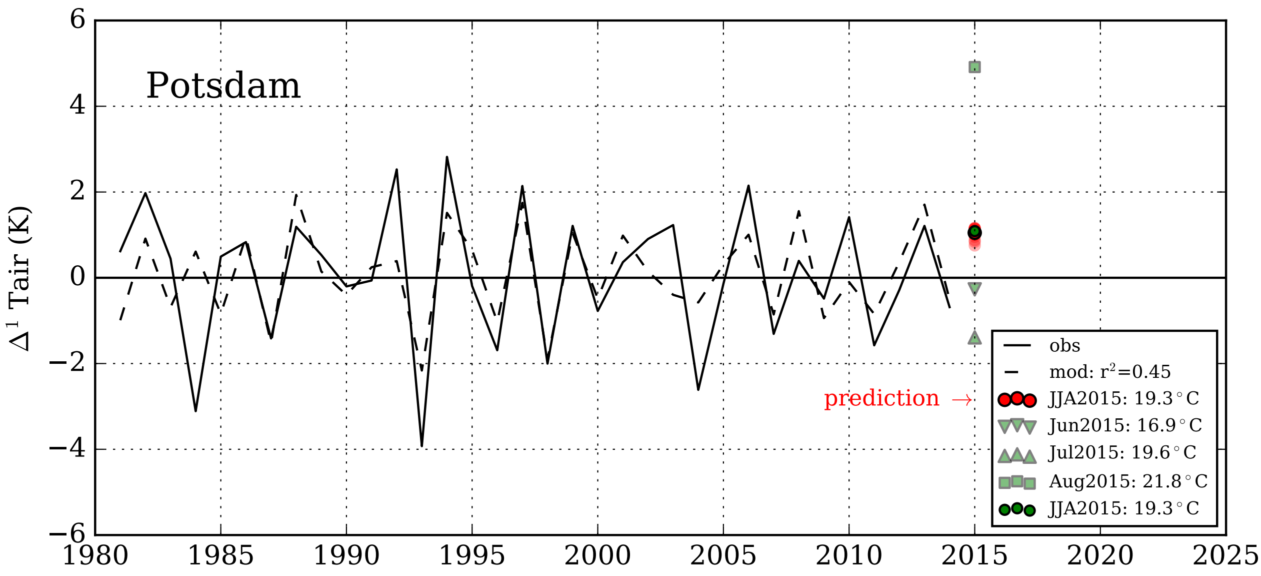

Fig. 3 Time series of the observed summer mean temperature (solid line) and the modeled one (dashed line) in Potsdam from 1981 to 2014 ($\triangle^1$). The out of sample prediction of 2015 (JJA2015, red) and the observed value (JJA2015, green) are given as scatter.. The individual monthly mean temperature means for June (Jun2015), July (Jul2015) and August (Aug2015) are shown as green triangles.

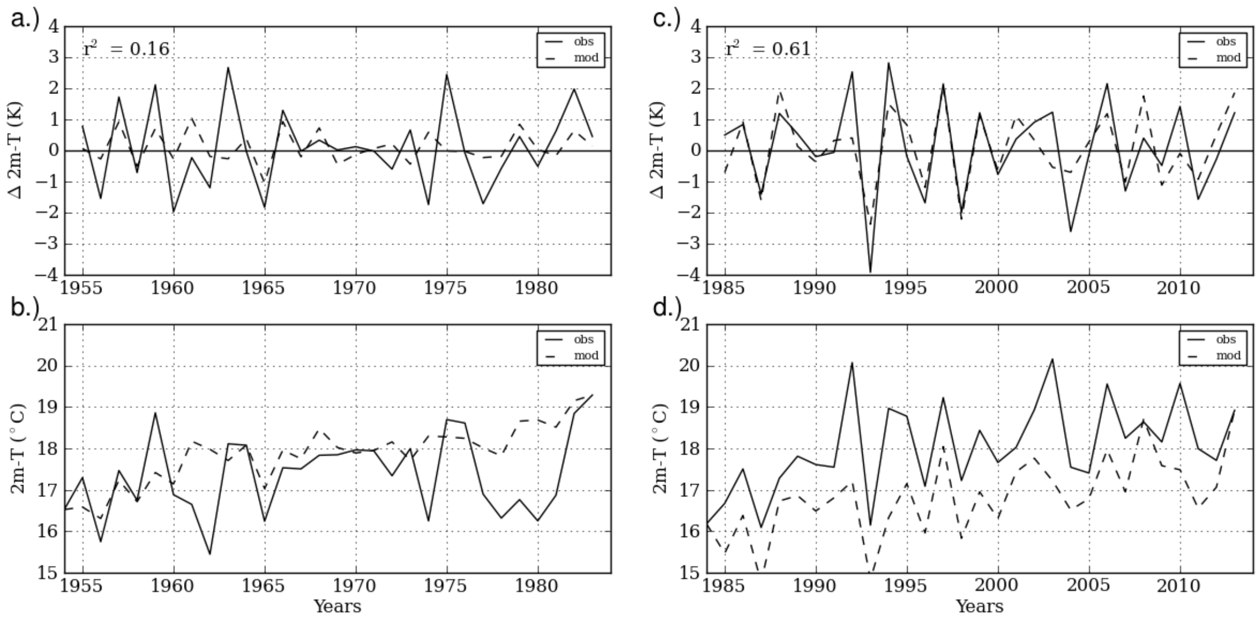

Fig. 4 Time series of the summer mean temperature ($\triangle^1$) at Potsdam observed (solid line) and simulated (dashed line) for two periods: 1954-1983 (a, b) and 1985-2014 (c, d). The corresponding absolute values are given in the lower row, respectively.

Although, the used first order differences are difficult to interpret with respect to absolute values, the relation to the previous year is better assessable. Figure 4 shows the model results applied to two periods 1955-1984 (left column) and 1985-2014 (right column). The lower row in Fig.4 depicts the re-calculated absolute values by using initial temperatures of the years 1954 and 1984, respectively. The comparison indicates a weak predictability measure for the early period (left column, $r^2 = 0.16$) compared to the late one (right column, $r^2 = 0.61$). However, a difference between the observed and the parallel simulated values of about -1K is evident for the last period. The absolute values in the late period are warmer and show a stronger year-to-year variability which is captured qualitatively well by the model. A much more systematic behavior can be seen by visualizing the whole parameter space using parallel coordinates (e.g. Inselberg, 1985). Figure 5 depicts the cumulated contributions of the predictors from January to April to the target value (T_{JJA}). Years, where T_{JJA} ($\triangle^1$) is lower/larger than -0.5K/0.5K are given in blue/red lines, respectively. About 65% of the years have a significant difference to the previous year. Almost no contributions of the early season predictors are found for the period 1955-1984 (left panel). All red and blue lines from January to April are close together. A few decades later the situation has changed. For the period 1985-2014 (right panel) we find much stronger contributions to the target value already in February, March and April. A clear spreading between the red and blue branch is evident (see Fig.5).

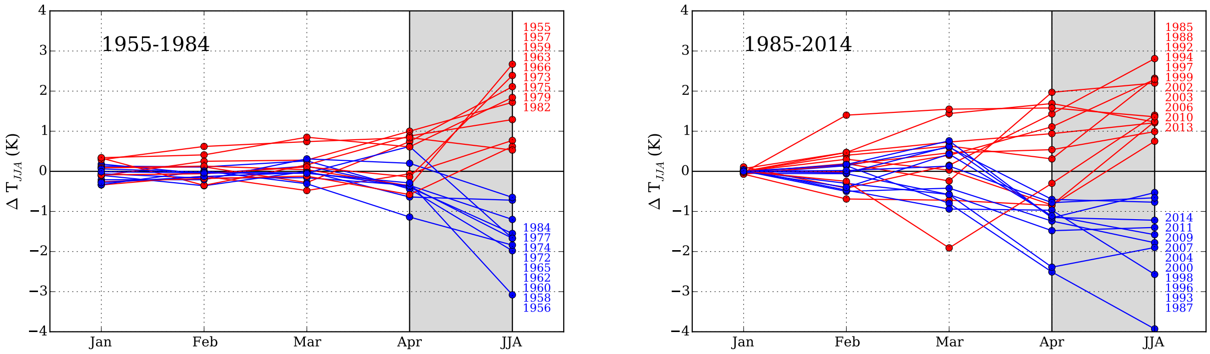

Fig. 5 Contributions of the monthly regression coefficients (January to April) to the target value (T_{JJA}) for two periods: 1955-1983 (left panel) and 1986-2014 (right panel). The blue/red lines show the preconditions for negative/positive summer mean temperature $\triangle^1$.

The long-term analysis of the predictability was done systematically applying this univariate regression model on time windows of 30 years, each shifted by one year, through the entire time series since 1893 (see Fig.6, top). The best model statistics were found for the last period 1985-2014 ($r^2 = 0.65$). Few decades before the model performance revealed a much lower predictability ($r^2 = 0.1 \ldots 0.3$). Around 1990 a state change from lower to higher seasonal predictability is evident. The graph for the one out-of-sample R-squared values (q^2) is clearly weaker and measures the predictability of the missing years. Such an increase of the seasonal predictability was already reported by Kang et al (2006) using climate data of the 20th century from the (C20C) AGCM experiment. The contributions of the individual coefficients (see Fig.6, bottom) indicate a regime shift around the year 1990 towards negative contributions.

3.2 Regional (Europe)

In order to investigate the predictability of the meteorological summer mean temperature (T_{JJA}) on the regional scale the model has been applied to the daily gridded dataset EOBS-0.25-v12.0 (Haylock et al, 2008) that is provided up to the year 2014. Every single grid point is thereby considered as an independent record. The observation period was subdivided into an early and a recent period and the derived predictability measures (r^2) were visualized. Figure 7 shows the distribution of the r^2-values over Europe for two periods: 1955-1984 (left panel) and 1985-2014 (right panel). The figure depicts when and where the regression model works well. High predictability is given in red color. This is the case for the recent period over the southern part of the Baltic region. Two secondary maxima are also visible for the Iberian Peninsula and Turkey. Due to the scarce data coverage and poor data quality over Turkey the signal is somewhat questionable. The other two patterns (Fig.7, right panel) are dataset independent and can be qualitatively reproduced using NCEP/NCAR R1 (Kalnay and et al., 1996) reanalysis data (Fig.15, Annex). Therein we also find another predictability maximum over Pakistan. However, this is beyond our interest. Low predictability is found over Western- and Eastern Europe for the late period and for whole of Europe in the middle of the last century. The r^2-values are clearly less than 0.3. The prominent differences between the two patterns require an investigation of circulation patterns over Europe and their long-term behavior.

An alternative approach was checked using Partial Least-Square (PLS) regression (Geladi and Kowalski, 1986) to predict the T_{JJA} at Potsdam based on February-April averaged NCEP/NCAR patterns of Δ^1Z500 over the Atlantic-European Sector (30.0°W–42.5°E/25.0°N–65.0°N). It is based on a principle component regression. Compared to Eq.1 the temporal fluctuations explained by the standard deviations are here expressed by the first two Δ^1Z500 principle components. This approach can qualitatively reproduce our results for the recent period (1991-2015) with $r^2 = 0.74$ (Fig.16, Annex). The simulation of an earlier period from 1971-1990 by using the resulting coefficient matrix failed, because the Δ^1Z500 patterns and their year-to-year variability must include structural differences compared to the recent period. This is an indirect way to detect circulation changes in the atmosphere for specific applications.

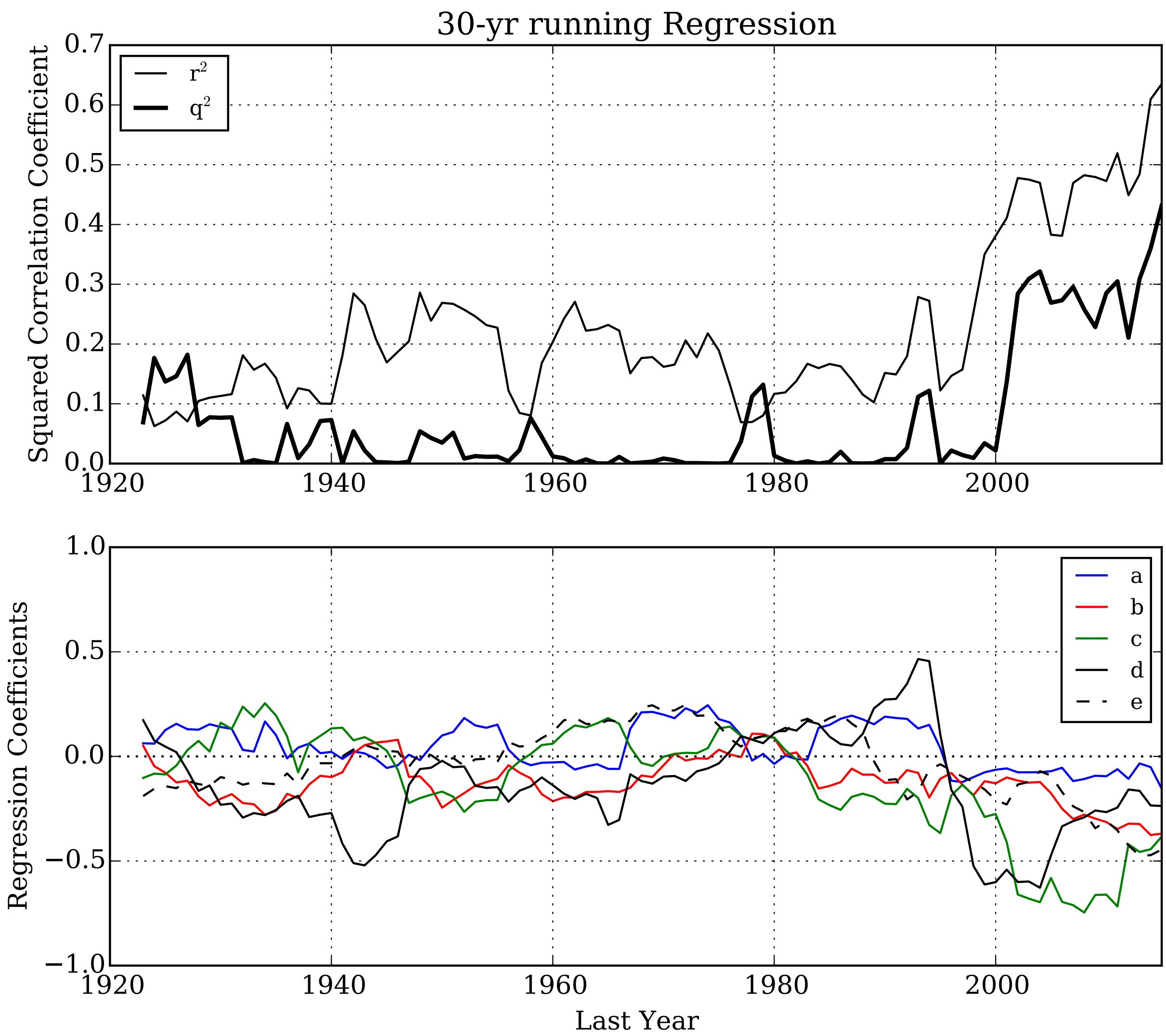

Fig. 6 *Upper panel:* Time series of the 30-years running squared correlation coefficients (r^2 and q^2) between the observed and modeled data from 1923 to 2014. *Lower panel:* Time series of the regression coefficient according to Eq.1.

3.3 Cross-Validation

The ability of the diagnostic model (Eq.1) for prediction purposes was evaluated by using the Leave-One-Out Cross-Validation (LOOCV) approach (Fig.8, upper right). This figure shows the already discussed R^2-value (blue line) and the RMSE between the predicted and the observed values (red line) for the Potsdam station. Thereby, the period from 1950 to 2016 was analyzed using a 30-year running time window. The two curves indicate opposite tendencies with clear jumps to enhanced predictability in recent years. The RMSE reaches values of about 0.9K. This is below the natural variability. Figure 8 (lower left) assess the prediction of the subsequent years. Every single scatter in the observed-forecast diagram indicates one prediction. A perfect forecast must be in line with the slant. The predicted $\Delta^1 T_{JJA}$ values since 2010 are given in red color. All last 6 forecasts were within the uncertainty band ($\pm 1K$). The last 3 years (2014, 2015, 2016) even very close to the slant. In order to assess the predictability skill on the regional scale the RMSE must be lower than the $1\sigma\,(T_{JJA})$. The hashed area in Fig.8 (right panel) fulfills this criteria. It is similar to the R^2-pattern (Fig.7, right panel). Consequently, recent predictions of $\Delta^1 T_{JJA}$ using Eq.1 for grid cells within the hashed areas are more reliable than the rest.

3.4 Dynamical (Europe)

The reason for the shown rising of the predictability measure is probably linked to a change in the circulation over Europe. Kyselý and Huth (2006) detected changes in the persistence of anticyclonic weather types in summer after 1990 using subjective and objective methods. They explain these changes by the northward shift of the storm track in the

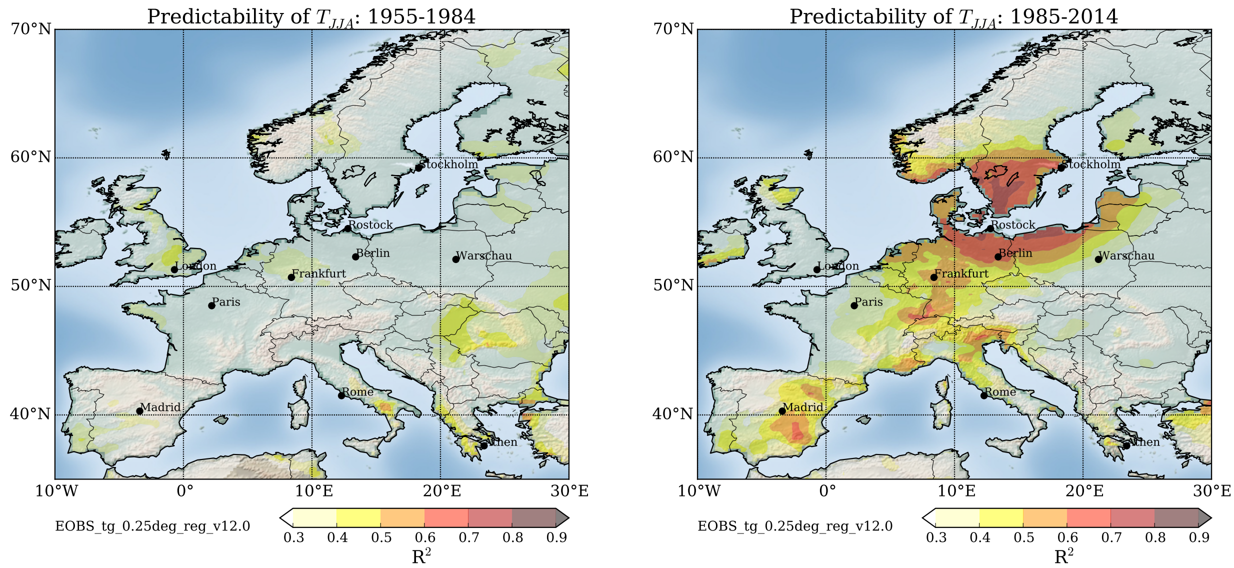

Fig. 7 European patterns of the squared-correlation coefficient (r^2) for two periods: 1955-1984 (left panel) and 1985-2014 (right panel). The location of Potsdam is represented by the red circle.

Northern Hemisphere. The related decrease of cyclonic activity and enhanced blocking frequency favor the predictability on the longer timescale. Here, we use a long-term (subjectively derived) catalog of weather patterns *(Grosswetterlagen)* after Hess and Brezowsky (1977) provided by the German Meteorological Service to identify possible changes in the occurrence frequency from 1961 to 2015. This classification relies on the synoptical experiences of meteorologists, which cannot be completely automated or discriminated objectively (James, 2007). Automated classifications of 40 weather type (e.g. Bissolli and Dittmann, 2001) are only available continuously since 1979 and are not considered in this study, because their reliability rises and falls with the used reanalysis dataset. Figure 9 shows the long-term monthly average of the 30 weather types (left panel) and their respective relative trends (right panel). The most frequent ones are the *Cyclonic Westerly* (WZ: 170 days/year) and the *Zonal-Ridge over Central Europe* (BM: 113 days/year). To the second most frequent group with more than 60 days/year belongs *High over Central Europe* (HM: 62 days/year) and *Trough over Central Europe* (TRM: 63 days/year). Two of these, BM and TRM, show a strong positive trend of the frequency in the summer half-year. Werner et al (2008) reported an increase of BM weather type during the summer months (June-August) already. All other weather types are either decreasing in frequency or their trends are not significant ($p > 0.05$). The BM and TRM patterns are often associated with a strong contrast of weather variables (Z500, SLP, surface temperature, precipitation, etc.) in Central Europe. Figure 10 (top) represents the respective shape of the circulation in the middle troposphere (Z500) for the two conditions. Both shapes show a strong dissimilarity to the other *Hess/Brezowsky* weather types. Their uniqueness makes a mistake in the classification process less likely. The distance between the two patterns ($Z500_{HB} - Z500_{TRM}$), *Zonal-Ridge* and *Trough over Central Europe*, is shown in Fig.10 (bottom). It reveals a core region, where the contrast between the two circulation types is large. This is the case for the north-eastern part of Central Europe and the Potsdam climate station is located in the center.

The temporal evolution of the two *Hess/Brezowsky* weather types since 1961 is shown in Fig.11. It represents their rising contributions on the total variability from March to July. While their percentage before 1980 laid below 10%, the conditions have changed after 1980. Their share has doubled and amounts currently almost 30%. This finding demonstrates that the variability of the chaotic weather system shifts to a more regular state determined by less degrees of freedom or in synoptical terminology, weather types. However, theses changes have side effects. The new dominant weather patterns favor weather extremes in the summer half-year: BM (heat waves) and TRM (heavy rainfall). The airflow is stronger meridional oriented.

An additional Fig.14 (Annex) illustrates the 15-30d bandpass filtered temperature values at Potsdam (red curve) given in polar coordinates for two years, 2014 (left panel) and 2015 (right panel). The occurred weather types, BM (red circle) and TRM (blue circles) are also added. It implies the live cycle of the new dominant weather patterns in comparison to the temperature variability, where TRM/BM favors negative/positive anomalies, respectively.

A used Mother-Wavelet analysis (Torrence and Compo, 1998) of the Potsdam temperature record (see Fig.12, left) also revealed a shift from a stronger seasonal variability ($\sim$ 50 days) in the early period to a prominent monthly variability ($\sim$ 30 days) in the recent period. Both, late winter (Jan-Mar) and spring (Apr-Jun) show synchronizing tendencies in this direction (see Fig.12, right). Weather patterns with high persistence potentials, such as BM and TRM, could trigger

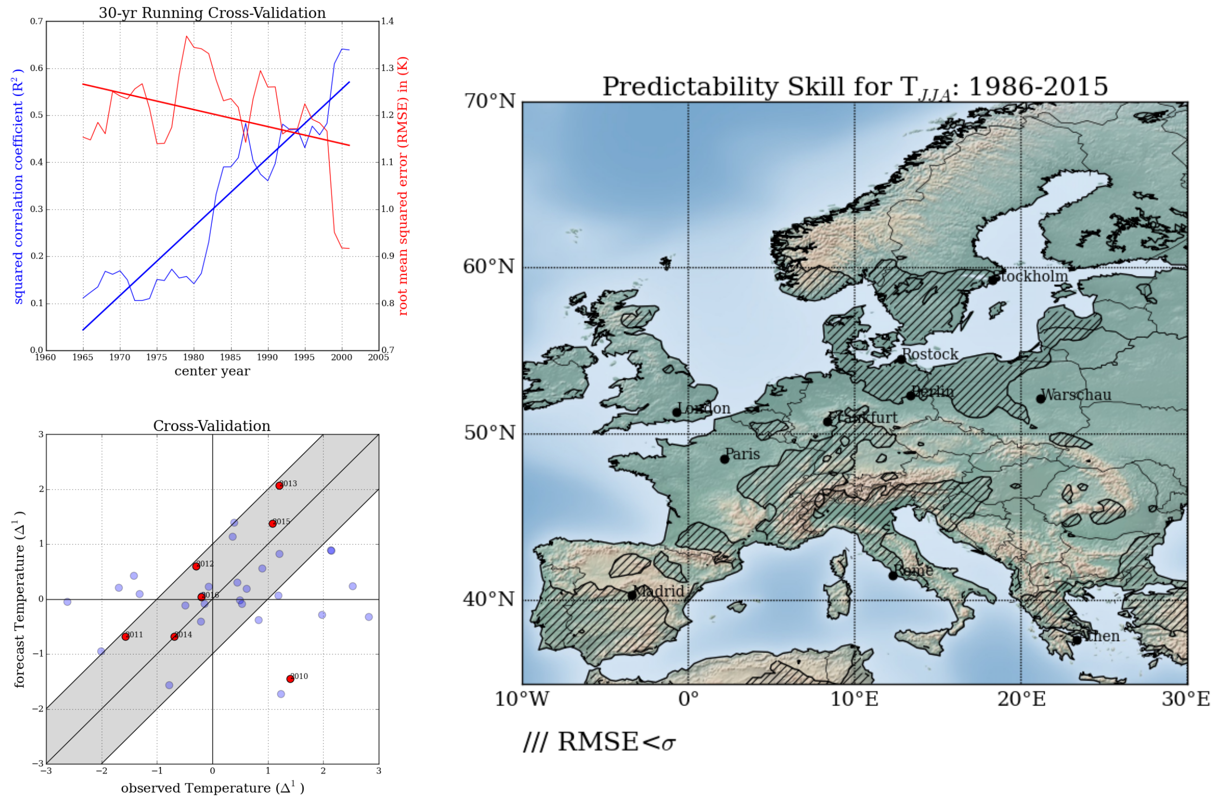

Fig. 8 Cross-validation: *upper left:* R^2- & $RMSE$-curve between model and observation for Potsdam. The trend lines are added, respectively. *lower left:* Observed-forecast diagram of $\Delta^1 T_{JJA}$ in Potsdam. The scatters represent predictions of the subsequent year. The predictions since 2010 are given in red. *right panel:* European map gives of the predictability skill (hashed areas) for $\Delta^1 T_{JJA}$ under recent climate conditions (1986-2015) where $RMSE < \sigma$.

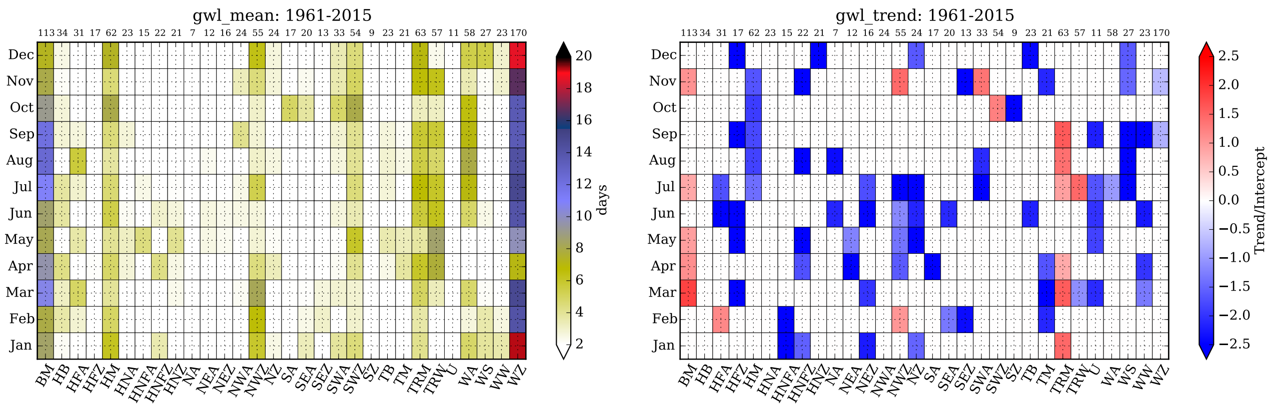

Fig. 9 1961–2015 long-term means (left panel) and relative trends (right panel) of *Hess/Brezowsky* weather types occurrences. Only significant trends with $p < 0.05$ are shown.

the inter-seasonal connectivity. This is also visible in the correlation matrices. These show coherent structures of such links derived from temperature (Fig.2) and weather type occurrences (Fig.13) by month. Different connection paths can be identified. The strongest change in the correlation is found for the BM and TRM weather types in the summer half-year (April-September). An obvious anti-correlation (blue scaling) determines the recent conditions (1986-2015). This alternation is not visible in the early period (1951-1980). Consequently, the patterns under recent conditions reveals more regularities and may confirm our findings for an enhanced seasonal predictability of the summer mean temperature in Central Europe favored by new dominant weather patterns.

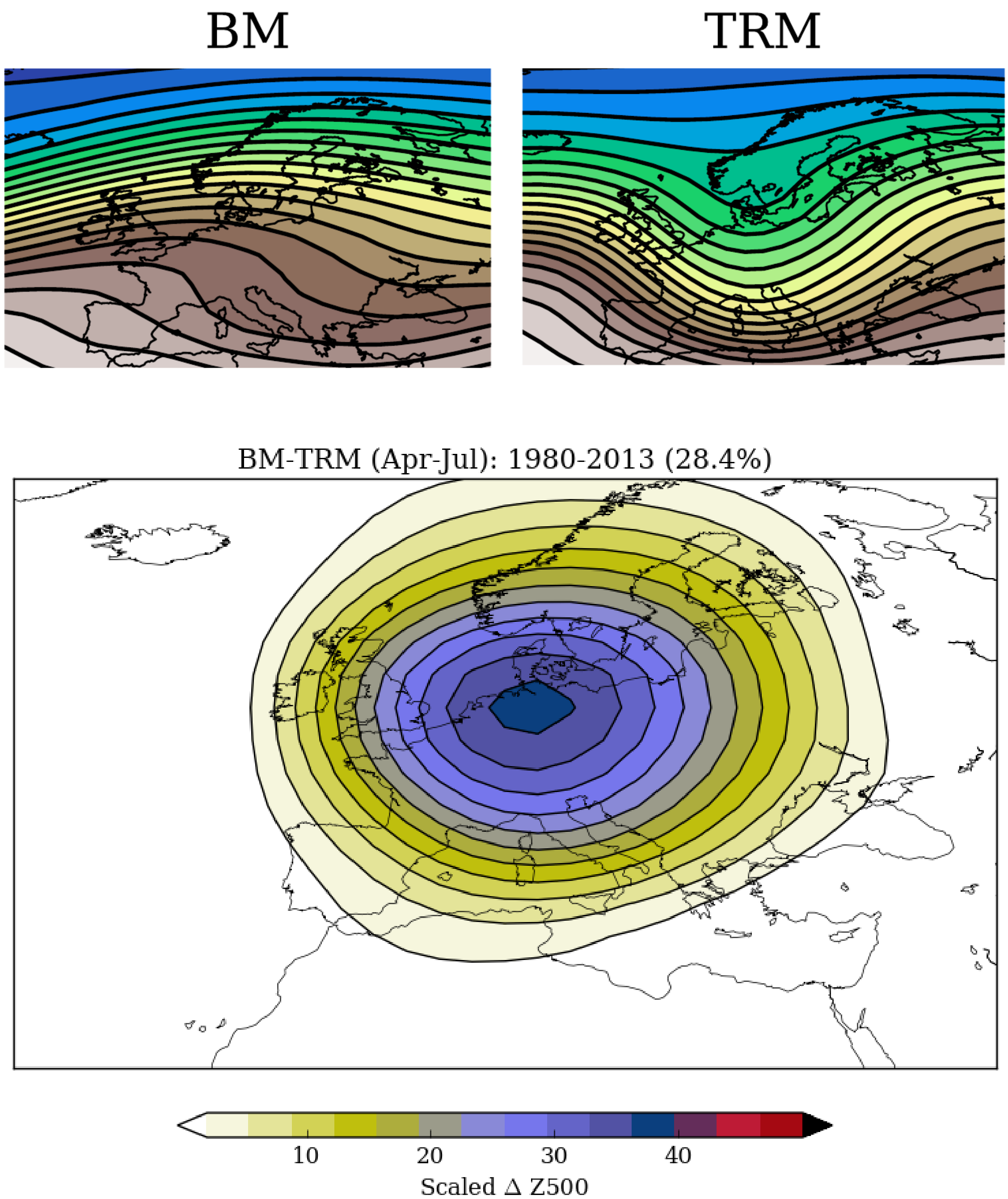

Fig. 10 *upper row:* Composite patterns of the re-scaled Z500 values in NCEP/NCAR reanalysis (Kalnay and et al., 1996) data for two *Hess-Brezowsky* weather types: BM (left) and TRM (right). *lower row:* Difference pattern of the two Z500 composites.

4 Conclusions

The seasonal predictability of the meteorological summer mean temperature (T_{JJA}) over Central Europe has improved during the last decades. This could be shown by using an empirical relation between the target value and early season predictors (late winter variability). A stronger year-to-year variability is evident and a linkage to the winter circulation through planetary wave activity (e.g. Zhang et al, 2014) was suggested. This was verified by using two complementary approaches analyzing *daily temperature records* and the occurrences of *Grosswetterlagen*. Both approaches came to similar results. (1) the circulation has changed after 1990, (2) the system shifts to a more regular and predictable state, (3) the strongest relation was found for the north-eastern part of Central Europe. We conclude that the spatial center of higher seasonal predictability was found at location where the distance of the prevailing weather types (BM and TRM) is large. Both weather types are usually associated with opposite weather conditions and reveal a stronger contribution to the total variability over Europe after 1990.

The sequence of BM and TRM can be interpreted as wave-like patterns of the jet stream over Europe. Thereby, the wave ridge and trough over Central Europe corresponds to the BM and TRM weather types. This finding provides an indirect

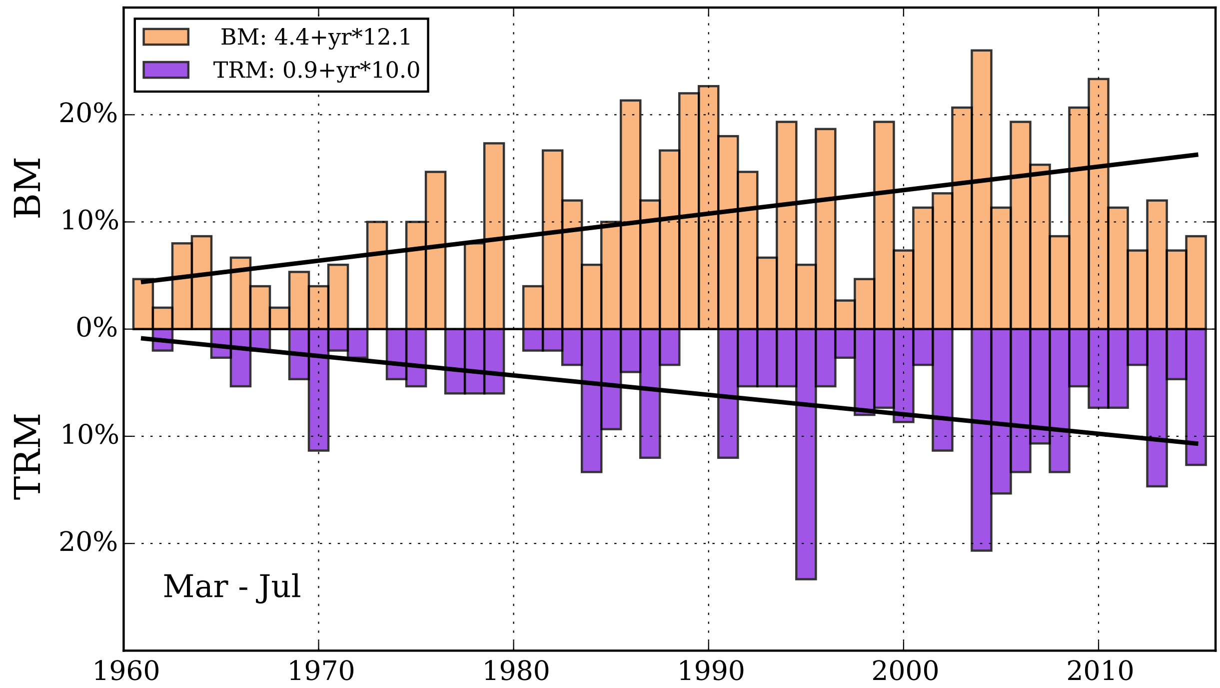

Fig. 11 1961–2015 long-term evolution of the contribution on the total variability for the two *Hess/Brezowsky* weather types from March to July: BM (sandybrown) and TRM (blueviolet). The individual trends are given as black lines.

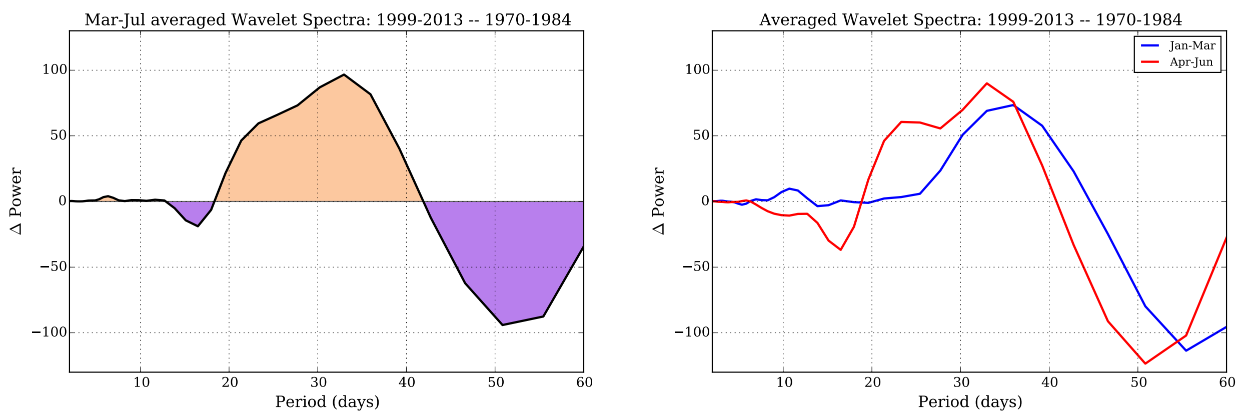

Fig. 12 *Left panel:* March to July averaged Mother-Wavelet spectra differences between two periods derived from the Potsdam temperature record: 1970–1984 and 1999–2013. *Right panel:* The same as above for Jan-Mar (blue line) and Apr-Jun (red line).

way to identify possible circulation changes by analyzing the local variability in daily temperature time series (winter) as early season predictors for a later temperature state (summer). The application of this approach to other temperature derived indices, such as the number of *hot days* ($T_{max} > 30$°C) provides similar results, even though the predictability measure is weaker (not shown).

In the context of climate change and the linkage to the Arctic amplification (e.g. Francis and Vavrus, 2012; Cohen et al, 2014) possible circulation changes during boreal summer at mid-latitudes are discussed by, e.g., Coumou et al (2014). A higher frequency of quasi-resonant circulation regimes will lead to more extreme weather events (droughts, heat waves or floods). This is, to a certain degree, consistent with our findings on the local and regional scale over Central Europe. Two weather pattern, which are often associated with extreme weather situations (BM: *droughts*, *heat waves* and TRM: *floods*) become more frequent and determine increasingly the variability of the chaotic weather system over Europe. The resulting enhanced predictability measure goes along with a higher probability of persistent extreme weather events in the summer half-year. This *side effect* is alarming and points towards more frequent extreme weather conditions in the further course of the rapid climate change.

Changes in the land-ocean temperature contrast in Northern Hemisphere (zonally asymmetric forcing) may also contribute to the enhanced predictability. In Jain et al (1999) detected changes in the seasonality of the land-ocean ratio

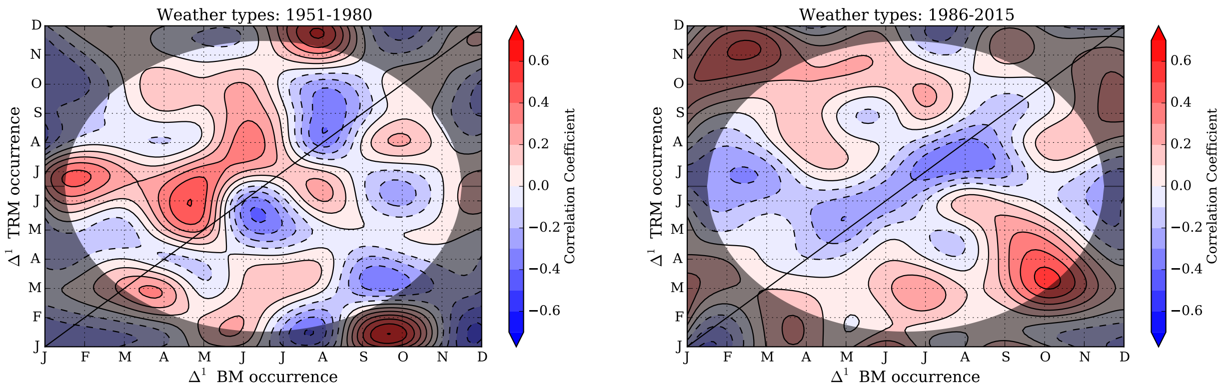

Fig. 13 Monthly Pearson correlation coefficient matrix between BM vs. TRM occurrence using $\triangle^1$ from 1951-1980 (left panel) and 1986-2015 (right panel). The area of interest is highlighted.

and the equator-pole gradient in historical data and one GCM run. Both parameters effect the large-scale circulation and the planetary scale variability (e.g. Molteni et al, 2011; Cohen et al, 2012). An impact of the land-ocean thermal contrast on blocking was studied by He et al (2014). They found more persistent events during positive phases of the Land-Sea Index (LSI) "cold land/warm ocean" in winter. However, long-term trends indicate a decrease of the blocking frequency due to the weakening of the LSI. We conclude, a possible connection to the enhanced seasonal predictability is likely.

The prediction of the summer mean temperature of 2016 in Potsdam was successful, too, as shown in Fig.8 (lower left panel). The estimated value of 19.1°C was hit exactly. The r^2-value for the training period 1994-2015 amounted to 0.62. Another temperature-based target value (the number of hot days) was estimated analogue to the described approach. Again, the estimated value of 15 days was hit exactly ($r^2 = 0.58$). Finally, the summer 2016 in Potsdam was similar compared to the previous year 2015 in terms of the mean temperature (19.3°C). However, $T_{max} > 30$°C was exceeded 11 times during the summer months June to August. Quite unusual, 4 more were reported in early September. That is altogether 10 days less than in 2015. The application for whole Europe was not realized due to missing real-time data.

For future work we plan to extend the prediction to other relevant parameters, such as total precipitation, by using a temperature conditioned weather generator. This allows to estimate how far dry or wet conditions during summer are favored by the predicted temperature state. Also a climate model assessment in terms of seasonal predictability over Europe is planned in order to evaluate their performances.

The application of a similar regression model to study the predictability skill for the winter season is much more complex. Folland et al (2012) described how potentially predictable is northern European winter climate a season ahead. They conclude that process-based forecast models must fully resolve the stratosphere dynamics and data-based approaches have to consider a much higher number of independent early season predictors (e.g. the North Atlantic SST index, QBO, Volcanic- and Nino 3.4 index).

Acknowledgements I thank Frank Wechsung for his critical comments during time preparing the manuscript and the German Meteorological Service for maintaining such a consistent climate record.

Supplementary Material

The supplementary materials include additional figures, which underline our general findings and the discussed mechanism.

S-Tab. 2 Prediction summary for Potsdam: mean temperature Jun-Aug (T_{JJA}), mean temperature Jul-Aug (T_{JA}) and hot days (hoda).

	observation					prediction			
	2014	2015	Δ^1	2016	Δ^1	2015	r^2	2016	r^2
ja						1986		1987	
T_{JJA}	18.2°C	19.3°C	+1.1K	19.1°C	-0.2K	**19.3°C**	0.64	**19.1°C**	0.63
T_{JA}	18.9°C	20.7°C	+1.8K	19.1°C	-1.5K	**20.7°C**	0.70	20.4°C	0.72
hoda	11d	21d	+10d	15d	-6d	**21.9d**	0.50	**15.2d**	0.52

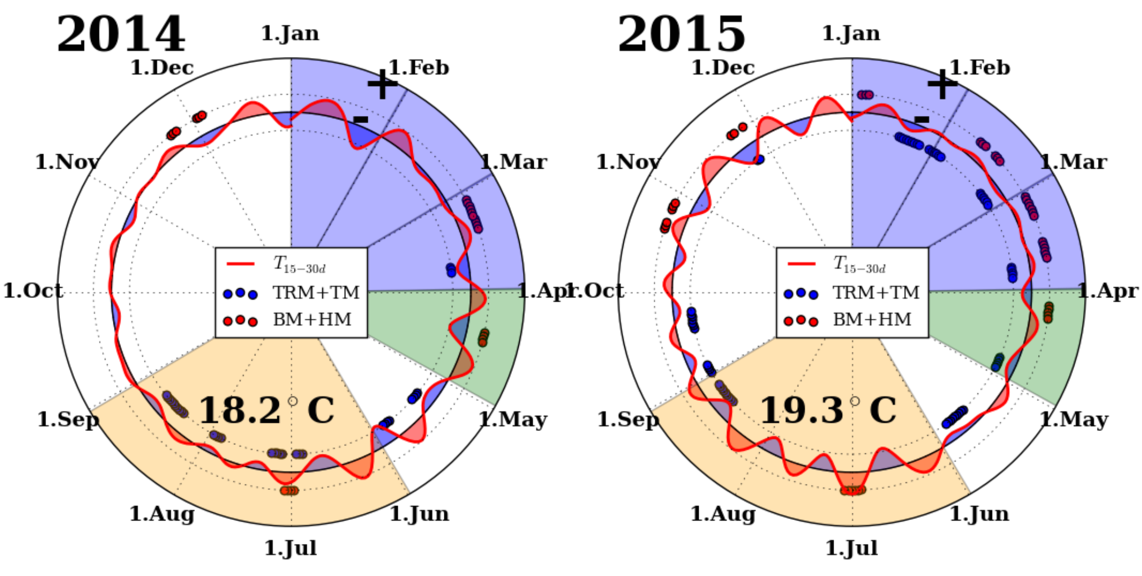

S-Fig. 14 Polar coordinates plots of 15-30d bandpass filtered temperature values at Potsdam (red lines) for the years 2014 (left panel) and 2015 (right panel). The different periods of the year are colored: January to March (blue), April (green) and June to August (orange). The occurrences of specific weather types are given as circles: TRM (blue) and BM (red).

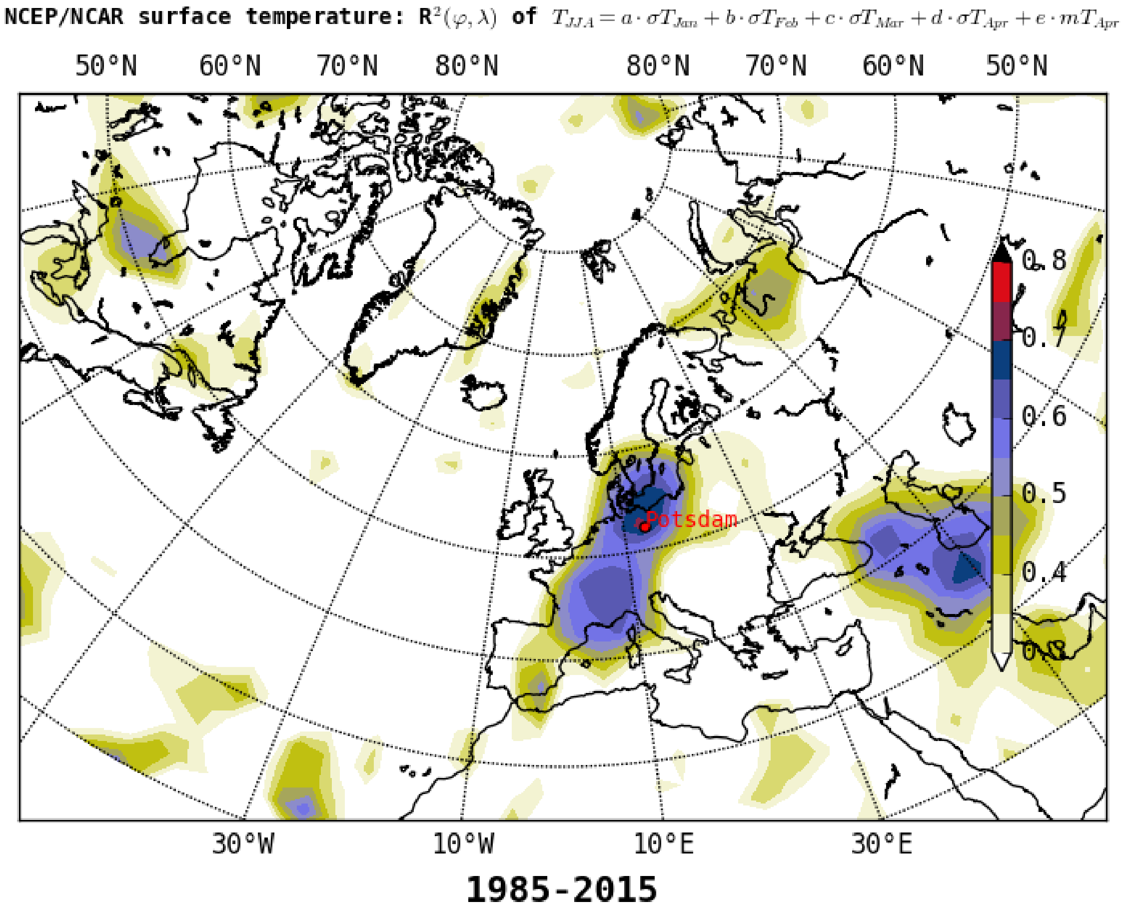

S-Fig. 15 European pattern of the squared-correlation coefficient (r^2) for the period 1985-2015 using near surface temperature data from NCEP/NCAR R1 (Kalnay and et al., 1996) analogue to Fig.7.

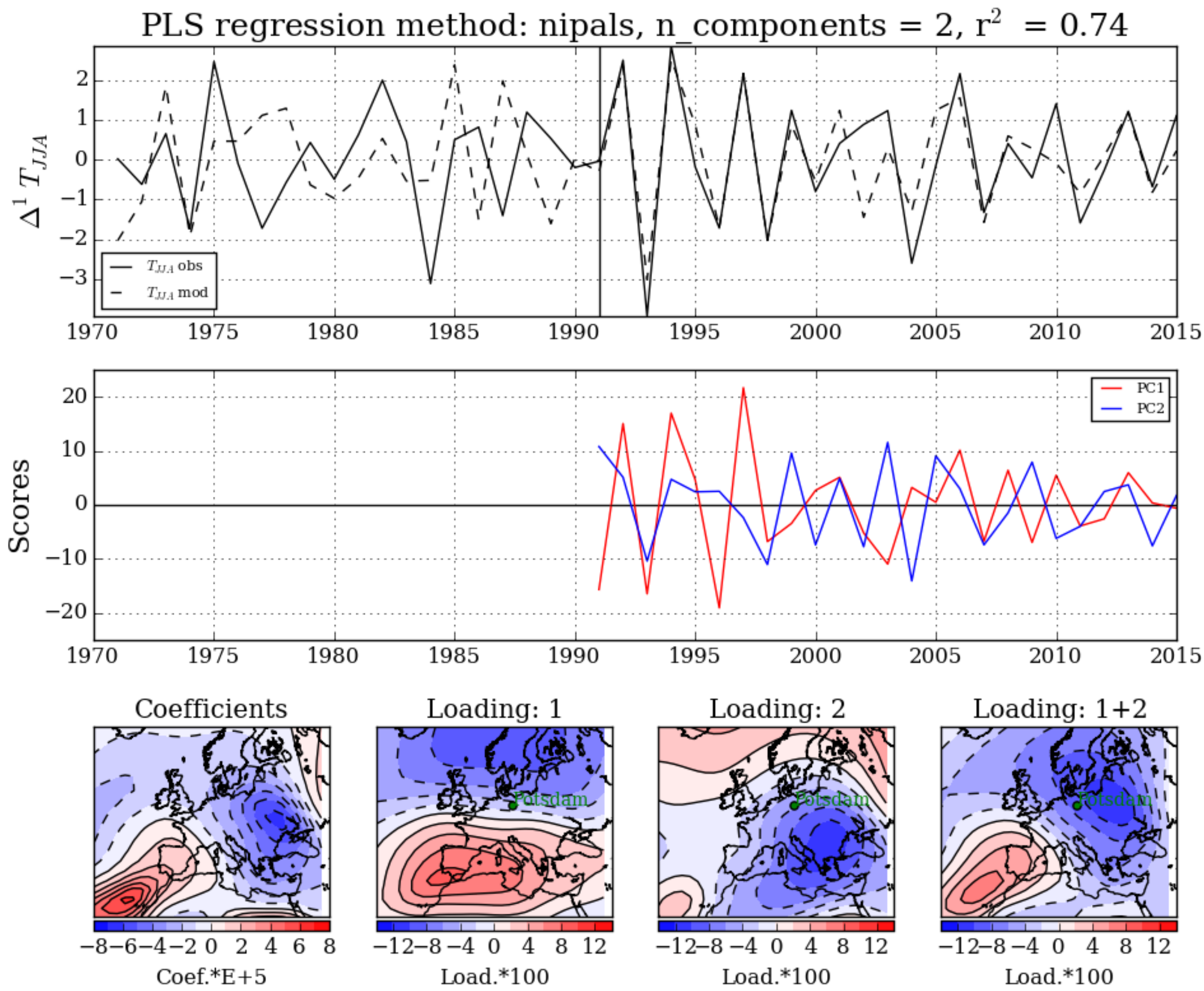

S-Fig. 16 Partial-Least-Squares (PLS) regression (black dashed) of the summer mean temperature at Potsdam (black solid) using Feb.-Apr. averaged Z500 patterns in NCEP/NCAR R1 reanalysis data over the Atlantic-European sector (top). The data are detrended using first differences ($\triangle^1$). The model was trained for the recent period (1991-2015) with $r^2 = 0.74$. The scores (middle) and patterns of the coefficients and loadings are added (bottom).

References

Barnett TP, Heinz HD, Hasselmann K (1984) Statistical prediction of seasonal air temperature over eurasia. Tellus A 36A(2):132–146, DOI 10.1111/j.1600-0870.1984.tb00233.x, URL http://dx.doi.org/10.1111/j.1600-0870.1984.tb00233.x

Barnston AG, Mason SJ (2011) Evaluation of iri's seasonal climate forecasts for the extreme 15% tails. Weather and Forecasting 26(4):545–554, DOI 10.1175/WAF-D-10-05009.1, URL http://dx.doi.org/10.1175/WAF-D-10-05009.1, http://dx.doi.org/10.1175/WAF-D-10-05009.1

Bissolli P, Dittmann E (2001) The objective weather type classi cation of the german weather service and its possibilities of application to environmental and meteorological investigations. Meteorol Z 10:253–260, DOI 10.1127/0941-2948/2001/0010-0253

Cohen J, Screen JA, Furtado JC, Barlow M, Whittleston D, Coumou D, Francis J, Dethloff K, Entekhabi D, Overland J (2014) Recent arctic amplification and extreme mid-latitude weather. Nature Geoscience 7(9):627–637, DOI 10.1038/ngeo2234

Cohen JL, Furtado JC, Barlow M, Alexeev VA, Cherry VA (2012) Asymmetric seasonal temperature trends. Geophys Res Lett 39:L04,705, DOI 10.1029/2011GL050582

Colman A, Davey M (1999) Prediction of summer temperature, rainfall and pressure in europe from preceding winter north atlantic ocean temperature. International Journal of Climatology 19(5):513–536, DOI 10.1002/(SICI)1097-0088(199904)19:5<513::AID-JOC370>3.0.CO;2-D, URL http://dx.doi.org/10.1002/(SICI)1097-0088(199904)19:5<513::AID-JOC370>3.0.CO;2-D

Coumou D, Robinson A, Rahmstorf S (2013) Global increase in record-breaking monthly-mean temperatures. Climatic Change 118(3):771–782, DOI doi:10.1007/s10584-012-0668-1

Coumou D, Petoukhov V, Rahmstorf S, Petri S, Schellnhuber HJ (2014) Quasi-resonant circulation regimes and hemispheric synchronization of extreme weather in boreal summer. PNAS 111(34):12,331–12,336, DOI 10.1073/pnas.1412797111

Della-Marta PM, Luterbacher J, von Weissenfluh H, Xoplaki E, Brunet M, Wanner H (2007) Summer heat waves over western europe 1880–2003, their relationship to large-scale forcings and predictability. Climate Dynamics 29(2):251–275, DOI 10.1007/s00382-007-0233-1, URL http://dx.doi.org/10.1007/s00382-007-0233-1

Eden JM, van Oldenborgh GJ, Hawkins E, Suckling EB (2015) A global empirical system for probabilistic seasonal climate prediction. Geoscientific Model Development 8(12):3947–3973, DOI 10.5194/gmd-8-3947-2015, URL http://www.geosci-model-dev.net/8/3947/2015/

Folland CK, Scaife AA, Lindesay J, Stephenson DB (2012) How potentially predictable is northern european winter climate a season ahead? International Journal of Climatology 32(6):801–818, DOI 10.1002/joc.2314, URL http://dx.doi.org/10.1002/joc.2314

Francis JA, Vavrus SJ (2012) Evidence linking arctic amplification to extreme weather in mid-latitudes. Geophys Res Lett 39:L06,801, DOI 10.1029/2012GL051000

Geladi P, Kowalski BR (1986) Partial least-squares regression: a tutorial. Analytica Chimica Acta 185:1 – 17, DOI http://dx.doi.org/10.1016/0003-2670(86)80028-9, URL http://www.sciencedirect.com/science/article/pii/0003267086800289

Gornott C, Wechsung F (2016) Statistical regression models for assessing climate impacts on crop yields: A validation study for winter wheat and silage maize in germany. Agricultural and Forest Meteorology 217:89 – 100, DOI http://dx.doi.org/10.1016/j.agrformet.2015.10.005, URL http://www.sciencedirect.com/science/article/pii/S0168192315007315

Haylock M, Hofstra N, Klein Tank A, Klok E, Jones P, New M (2008) A european daily high-resolution gridded dataset of surface temperature and precipitation. J Geophys Res 113:D20,119, DOI 10.1029/2008JD10201

He Y, Huang J, Ji M (2014) Impact of land–sea thermal contrast on interdecadal variation in circulation and blocking. Climate Dynamics 43(12):3267–3279, DOI 10.1007/s00382-014-2103-y, URL http://dx.doi.org/10.1007/s00382-014-2103-y

Hess P, Brezowsky H (1977) Catalog of the general weather situations of europe 1981-1976. German Meteorological Service

Inselberg A (1985) The plane with parallel coordinates. The Visual Computer 1(2):69–91, DOI 10.1007/BF01898350, URL http://dx.doi.org/10.1007/BF01898350

Jain S, Lall U, Mann ME (1999) Seasonality and interannual variations of northern hemisphere temperature: Equator-to-pole gradient and ocean-land contrast. Journal of Climate 12(4):1086–1100, DOI 10.1175/1520-0442(1999)012<1086:SAIVON>2.0.CO;2, URL http://dx.doi.org/10.1175/1520-0442(1999)012<1086:SAIVON>2.0.CO;2, http://dx.doi.org/10.1175/1520-0442(1999)012<1086:SAIVON>2.0.CO;2

James PM (2007) An objective classification method for hess and brezowsky grosswetterlagen over europe. Theor Appl Climatol 88:17–42, DOI 10.1007/s00704-006-0239-3

Jarlan L, Abaoui J, Duchemin B, Ouldbba A, Tourre YM, Khabba S, Le Page M, Balaghi R, Mokssit A, Chehbouni G (2014) Linkages between common wheat yields and climate in morocco (1982–2008). International Journal of Biometeorology 58(7):1489–1502, DOI 10.1007/s00484-013-0753-9, URL http://dx.doi.org/10.1007/s00484-013-0753-9

Kalnay E, et al (1996) The ncep/ncar 40-year reanalysis project. Bull Amer Meteor Soc 77:437–470

Kang IS, Jin EK, An KH (2006) Secular increase of seasonal predictability for the 20th century. Geophysical Research Letters 33(2):n/a–n/a, DOI 10.1029/2005GL024499, URL http://dx.doi.org/10.1029/2005GL024499, l02703

Knippertz P, Christoph M, Speth P (2003) Long-term precipitation variability in morocco and the link to the large-scale circulation in recent and future climates. Meteorology and Atmospheric Physics 83(1):67–88, DOI 10.1007/s00703-002-0561-y, URL http://dx.doi.org/10.1007/s00703-002-0561-y

Kyselý J, Huth R (2006) Changes in atmospheric circulation over europe detected by objective and subjective methods. Theoretical and Applied Climatology 85(1):19–36, DOI 10.1007/s00704-005-0164-x, URL http://dx.doi.org/10.1007/s00704-005-0164-x

Lehmann J, Coumou D, Frieler K (2015) Increased record-breaking precipitation events under global warming. Climatic Change 132:501–515, DOI http://dx.doi.org/10.1007/s10584-015-1434-y

Molteni F, King MP, Kucharski F, Straus DM (2011) Planetary-scale variability in the northern winter and the impact of land–sea thermal contrast. Climate Dynamics 37(1):151–170, DOI 10.1007/s00382-010-0906-z, URL http://dx.doi.org/10.1007/s00382-010-0906-z

Petoukhov V, Rahmstorf S S andPetri, Schellnhuber HJ (2013) Quasiresonant amplification of planetary waves and recent northern hemisphere weather extremes. Proceedings of the National Academy of Sciences of the United States of America 110(14):5336–5341, DOI 10.1073/pnas.1222000110

Prokoph A, Patterson RT (2004) Application of wavelet and regression analysis in assessing temporal and geographic climate variability: Eastern ontario, canada as a case study. Atmosphere-Ocean 42(3):201–212, DOI 10.3137/ao.420304

Rust HW, Richling A, Bissolli P, Ulbrich U (2015) Linking teleconnection patterns to european temperature - a multiple linear regression model. Meteorologische Zeitschrift 24(4):411–423, DOI 10.1127/metz/2015/0642, URL http://dx.doi.org/10.1127/metz/2015/0642

Saha S, Coauthors (2014) The NCEP Climate Forecast System Version 2. Journal of Climate 27:2185–2208, DOI http://dx.doi.org/10.1175/JCLI-D-12-00823.1

Smoliak BV, Wallace JM, Stoelinga MT, Mitchell TP (2010) Application of partial least squares regression to the diagnosis of year-to-year variations in pacific northwest snowpack and atlantic hurricanes. Geophysical Research Letters 37(3):n/a–n/a, DOI 10.1029/2009GL041478, URL http://dx.doi.org/10.1029/2009GL041478, l03801

Stock JH, Watson MW (2002) Forecasting using principal components from a large number of predictors. Journal of the American Statistical Association 97(460):1167–1179

Torrence C, Compo GP (1998) A practical guide to wavelet analysis. Bull Amer Meteor Soc 79:61–78, DOI 10.1175/1520-0477(1998)079

Träger-Chatterjee C, Müller RW, Bendix J (2014) Analysis and discussion of atmospheric precursor of european heat summers. Advances in Meteorology 2014(427916), DOI 10.1155/2014/427916

Werner P, Gerstengarbe FW, Wechsung F (2008) Grosswetterlagenwetterlagen and precipitation trends in the elbe river catchment. Meteorologische Zeitschrift 17(1):061–066, DOI 10.1127/0941-2948/2008/0263

Wold S, Sjöström M, Eriksson L (2001) Pls-regression: a basic tool of chemometrics. Chemometrics and Intelligent Laboratory Systems 58(2):109–130, DOI 10.1016/S0169-7439(01)00155-1

Zhang YL, Liu Y, Chuan-Xi (2014) Dynamic seasonal transition from winter to summer in the northern hemisphere stratosphere. Atmospheric and Oceanic Science Letters 7(3):180, DOI 10.3878/j.issn.1674-2834.13.0082, URL http://159.226.119.58/aosl/EN/abstract/article_436.shtml